On the equal-mass limit of precessing black-hole binaries

2017 Class. Quantum Grav. 34 064004

(http://iopscience.iop.org/0264-9381/34/6/064004)

OPEN ACCESS
IOP Publishing
Classical and Quantum Gravity
Class. Quantum Grav. **34** (2017) 064004 (13pp)
https://doi.org/10.1088/1361-6382/aa5e58

On the equal-mass limit of precessing black-hole binaries

Davide Gerosa[1,2,5], **Ulrich Sperhake**[1,2,3] **and Jakub Vošmera**[2,4]

[1] TAPIR 350-17, California Institute of Technology, 1200 E California Boulevard, Pasadena, CA 91125, United States of America
[2] Department of Applied Mathematics and Theoretical Physics, Centre for Mathematical Sciences, University of Cambridge, Wilberforce Road, Cambridge CB3 0WA, United Kingdom
[3] Department of Physics and Astronomy, The University of Mississippi, University, MS 38677, United States of America
[4] Institute of Physics AS CR, Na Slovance 2, Prague 8, Czechia

E-mail: dgerosa@caltech.edu

Received 20 December 2016, revised 25 January 2017
Accepted for publication 6 February 2017
Published 1 March 2017

Abstract

We analyze the inspiral dynamics of equal-mass precessing black-hole binaries using multi-timescale techniques. The orbit-averaged post-Newtonian evolutionary equations admit two constants of motion in the equal-mass limit, namely the magnitude of the total spin S and the effective spin ξ. This feature makes the entire dynamics qualitatively different compared to the generic unequal-mass case, where only ξ is constant while the variable S parametrizes the precession dynamics. For fixed individual masses and spin magnitudes, an equal-mass black-hole inspiral is uniquely characterized by the two parameters (S, ξ): these two numbers completely determine the entire evolution under the effect of radiation reaction. In particular, for equal-mass binaries we find that (i) the black-hole binary spin morphology is constant throughout the inspiral, and that (ii) the precessional motion of the two black-hole spins about the total spin takes place on a longer timescale than the precession of the total spin and the orbital plane about the total angular momentum.

Keywords: black holes, gravitational waves, post-Newtonian theory

(Some figures may appear in colour only in the online journal)

[5] Einstein Fellow

1. Introduction

In the framework of general relativity, the dynamics of black-hole (BH) binaries and their emitted gravitational-wave (GW) signals are determined by the masses and spins of the inspiralling BHs. The binary's total mass $M = m_1 + m_2$ primarily sets the GW frequency, and therefore determines the required detection technique. Ground-based interferometers are sensitive to BH binaries with masses $\mathcal{O}(1-100)M_\odot$ [1, 2], space GW missions will be most sensitive to BHs of $M \sim \mathcal{O}(10^4 - 10^7)M_\odot$ [3], while Pulsar Timing Arrays target the detection of GWs from even more massive binaries of $\mathcal{O}(10^8 - 10^{10})M_\odot$ [4–6]. The mass ratio $q = m_2/m_1 \leqslant 1$ directly enters the BH dynamics and the quantity most accurately determined in observations of BH inspirals is the binary's chirp mass $M_c = M[q/(1+q)]^{3/5}$ which sets the phase of the emitted GWs [7, 8]. The BH spins $\mathbf{S_1}$ and $\mathbf{S_2}$, although more difficult to measure, also directly affect the GW signal. Specifically, the spin components aligned with the orbital angular momentum affect the coalescence time as more (if spins are aligned) or less (if spins are anti-aligned) angular momentum is shed before merger [9]. This effect may be viewed as part of general relativity's tendency to cloak spacetime singularities inside horizons according to Penrose's cosmic censorship conjecture [10, 11] as excessive angular momentum of the post-merger BH would imply a naked singularity. In the presence of non-vanishing spin components perpendicular to the orbital angular momentum, precession due to relativistic spin-spin and spin–orbit coupling introduces characteristic modulations in the emitted chirp [12, 13]. Future observation of these patterns may help in determining the formation channel of binary BHs [14–16]. The BH spins also play a crucial role in determining the final properties of the BH remnant [17–19], especially its recoil velocity [20–22]. In terms of gravitational-wave source modelling, BH spins increase the number of source parameters by six, significantly increasing the complexity of the systems; see, for instance, [23–26], also for attempts to simplify the task. It is highly desirable, in this context, to dissect, in so far as possible using analytic means, the complicated morphology of spin precession and classify its key features.

Spin precession influences the binary dynamics on timescales $t_{\rm pre} \propto r^{5/2}$ (where r is the binary separation) [12, 13]. In the post-Newtonian (PN) regime $r/M \gg 1$ and $t_{\rm pre}$ is (i) much longer than the orbital period $t_{\rm orb} \propto r^{3/2}$, and (ii) much shorter than the inspiral timescale $t_{\rm RR} \propto r^4$ [27]. The resulting hierarchy

$$t_{\rm orb} \ll t_{\rm pre} \ll t_{\rm RR} \tag{1.1}$$

turns out to be a very powerful tool to study the binary dynamics: different processes (namely orbital motion, precession and inspiral) can be modelled on their respective timescales by averaging over quantities varying on shorter times and keeping constant those variables that only evolve over the longer time scales. The resulting equations can then be reassembled as a complete formalism using a quasi-adiabatic approach. This idea is at the heart of the decades-old orbit-averaged formulation of the BH binary dynamics [12, 13, 27], as well as the new precession-averaged PN approach [28, 29].

In this paper, we complement the analysis of [28, 29] by studying in detail equal-mass systems ($q = 1$). At first glance, this may appear as a predominantly academic exercise, but it is also of practical importance for at least four reasons.

(i) As we will discuss at greater length below, the subset of $q = 1$ binaries behaves qualitatively different in several regards relative to the generic unequal-mass case studied in

[28, 29] because of the existence of an additional constant of motion (section 2.1). This phenomenon also manifests itself at a formal level: merely setting $q = 1$ in the mathematical framework developed in [28, 29] leads to singular expressions in various places and, hence, does not directly predict the dynamics of equal-mass binaries.

(ii) Even though the behaviour of $q = 1$ binaries is ultimately derived from the formalism developed in [28, 29], the emerging picture is of such remarkable simplicity that it serves as an ideal pedagogical introduction and motivation for readers to venture on to the more complex spin-precession formalism of the cited work.

(iii) During the first years after the numerical relativity breakthroughs [30–32] the majority of numerical BH studies focussed on equal-mass binaries and, to this day, equal-mass binaries have frequently been used as testbeds for BH evolutions [33–37]. This choice is quite natural for several reasons (for instance, the additional symmetry allows for reduced computational domains and the merger dynamics probe the most strongly non-linear regime), but it involves a small risk that observations made for this particular class of binaries be mistaken as generically valid. Our study provides a cautionary statement in this regard, as we indeed identify characteristic features that hold for equal-mass systems and *only* for equal-mass systems: the constancy of the total spin magnitude S and a difference in timescale between the precession of the individual spins and that of the orbital plane.

(iv) Vice versa, the extraordinarily simple behaviour of the equal-mass case may yield valuable insight into characteristic features of BH binaries that, while not exactly valid for $q \neq 1$, may still hold approximately and thus contribute to our understanding of general systems. For instance, if BH binaries with mass ratio reasonably close to unity are found, the additional constant of motion stressed in section 2.1 will still be conserved *in practice* at some approximate level and may thus be useful in the modeling of GW signals. We note, in this context, that the first GW observations are all compatible with equal-mass BH binary sources within a 90% credibility interval [38–41].

The remainder of this work is organized as follows. Our calculations are carried out in section 2; results are illustrated in section 3 and conclusions drawn in section 4.

2. Peculiarities of the equal-mass case

According to the spin-precession formalism developed in [28, 29], the evolution of the BH spins is conveniently split into dynamics occurring on the precession time scale $t_{\rm pre}$ and those happening on the much longer radiation reaction time scale $t_{\rm RR}$. A key simplification arises from the fact that the projection of the effective spin along the orbital angular momentum,

$$\xi = \frac{1}{M}\left(\frac{\mathbf{S_1}}{m_1} + \frac{\mathbf{S_2}}{m_2}\right)\cdot\hat{\mathbf{L}}, \tag{2.1}$$

is a constant of motion of the orbit-averaged 2PN spin-precession equations and 3.5 PN radiation-reaction equation [42, 43]; at this order, ξ is constant on both time scales $t_{\rm pre}$ and $t_{\rm RR}$. The binary dynamics on the precession time scale is parametrized by the magnitude S of the total spin $\mathbf{S} = \mathbf{S}_1 + \mathbf{S}_2$ while the secular evolution under the effect of radiation reaction is encoded into the total angular momentum $\mathbf{J} = \mathbf{L} + \mathbf{S}$. A schematic view of these vectors and the angles between them is shown in figure 1.

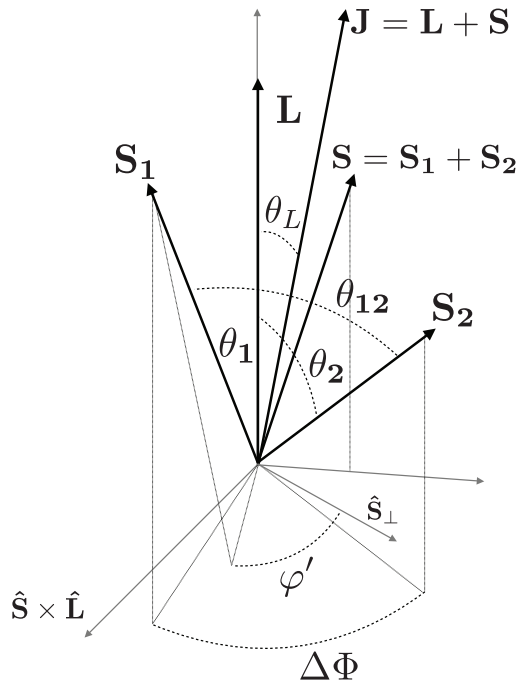

Figure 1. Vectors and angles describing the dynamics of spinning BH binaries. The directions of the two spins $\mathbf{S_1}$ and $\mathbf{S_2}$ with respect to the orbital angular momentum $\mathbf{L}$ are described in terms of the angles $\theta_\mathbf{1}$, θ_2, θ_{12} and $\Delta\Phi$, see equations (2.11)–(2.14). The orientation of the total angular momentum $\mathbf{J}$ relative to $\mathbf{L}$ is specified by the angle θ_L. The angle φ' used in section 2.2 to describe the spin dynamics is measured in the plane orthogonal to $\mathbf{S}$. The plane is orthogonal only to $\mathbf{S}$, in general not to $\mathbf{L}$.

2.1. Constants of motion

Constants of motion play a crucial role in this story. Let us consider an equal-mass BH binary, with mass ratio $q = m_2/m_1 = 1$ and total mass $M = m_1 + m_2$ on a quasi-circular orbit. The magnitudes of the BH spins $S_i = m_i^2\chi_i = M^2\chi_i/4$ $(i = 1, 2)$ are described in terms of the dimensionless Kerr parameter $0 \leqslant \chi_i \leqslant 1$, while the magnitude of the orbital angular momentum L is given (at the PN order here considered) in terms of the binary separation r by the Newtonian relation $L = m_1 m_2\sqrt{r/M} = \sqrt{rM^3}/4$. In this case, the effective spin projection ξ (2.1) becomes

$$\xi = 2\frac{\mathbf{S}\cdot\hat{\mathbf{L}}}{M^2} \quad \Rightarrow \quad |\xi| \leqslant \frac{2S}{M^2}. \tag{2.2}$$

Both the total angular momentum $\mathbf{J}$ and the magnitude of the orbital angular momentum L are constant on the precessional timescale $t_{\rm pre}$, because GWs only dissipate energy and momentum on $t_{\rm RR}$. The magnitude of the total spin S, on the other hand, may vary on $t_{\rm pre}$ under the effect of relativistic spin-spin and spin–orbit couplings and was used in [28, 29] to parametrize the precession dynamics for $q \neq 1$ binaries. It was noted, however, that there exist a few special configurations where S is constant, such as Schnittman's spin–orbit resonances [44] and stable binary configurations with aligned spins [45].

We find here the first qualitative difference in the behaviour of equal-mass binaries; for $q = 1$, the total spin magnitude S is *always* constant. This can be seen as follows. The standard orbit-averaged spin precession equations at 2PN order [12, 43] for $q = 1$,

$$\frac{\mathrm{d}\mathbf{S_1}}{\mathrm{d}t} = \frac{1}{2r^3}\left(7\mathbf{L} - \frac{3}{2}M^2\xi\hat{\mathbf{L}} + \mathbf{S_2}\right)\times\mathbf{S_1}, \tag{2.3}$$

$$\frac{\mathrm{d}\mathbf{S_2}}{\mathrm{d}t} = \frac{1}{2r^3}\left(7\mathbf{L} - \frac{3}{2}M^2\xi\hat{\mathbf{L}} + \mathbf{S_1}\right)\times\mathbf{S_2}. \tag{2.4}$$

imply $\mathrm{d}S^2/\mathrm{d}t = 2\mathbf{S}\cdot\mathrm{d}\mathbf{S}/\mathrm{d}t \propto \mathbf{S}\cdot\mathrm{d}(\mathbf{S}_1+\mathbf{S}_2)/\mathrm{d}t \propto \mathbf{S}\cdot(\mathbf{L}\times\mathbf{S}) = 0$. It follows that for all $q = 1$ configurations, the magnitude S is conserved on the precession and the radiation-reaction timescales [though not necessarily on the orbital timescale over which equations (2.3) and (2.4) are averaged]. This point was realized at least as early as 2008 in [43]. A similar conclusion had previously been reached in [13] with an incomplete set of 2PN equations and using some further assumptions. By cosine rule, the angle θ_L between orbital and total angular momentum satisfies $2JL\cos\theta_L = J^2 + L^2 - S^2$, so that with equation (2.2) and $\mathbf{J}\cdot\mathbf{L} = L^2 + \mathbf{S}\cdot\mathbf{L}$ we find

$$J = \sqrt{L^2 + S^2 + L\xi M^2}\,. \tag{2.5}$$

This relation holds on $t_{\rm pre}$ and, more importantly, on $t_{\rm RR}$ and therefore describes the evolution of J as the separation decreases under GW emission.

These results can also be found using the precession-averaged approach of [28, 29]: With $q = 1$, equation (13) of [29] gives

$$\xi = \frac{J^2 - L^2 - S^2}{M^2 L}, \tag{2.6}$$

and the effective potentials of BH spin precession, ξ_+ and ξ_-, coincide for $q = 1$, implying that S is constant on the precession time. The precession averaging in equation (38) of [29] then becomes a trivial operation, so that

$$\frac{\mathrm{d}J}{\mathrm{d}L} = \frac{J^2 + L^2 - S^2}{2LJ} = \frac{2L + \xi M^2}{2J} \quad\Rightarrow\quad 2J\,\mathrm{d}J = 2L\,\mathrm{d}L + \xi M^2\,\mathrm{d}L, \tag{2.7}$$

and after integration $J^2 - L^2 - \xi L M^2 = \text{const}$ on $t_{\rm RR}$. By equation (2.6), this constant must be S^2 and we have recovered equation (2.5).

Note the remarkable character of this finding. With $q = 1$ and chosen parameters S_1, S_2, BH binaries are specified by pairs (ξ, S): both these quantities are constant on the precession and radiation reaction time scale and uniquely determine the binary's characteristics. L is merely a measure for the binary separation r and J, the only evolving dependent variable, is determined by the simple analytic expression (2.5). All other properties of the binary, such as the mutual orientation of the BH spins and that of the orbital plane, follow from straightforward geometric considerations of the triangles $(\mathbf{J}, \mathbf{L}, \mathbf{S})$ and $(\mathbf{S}, \mathbf{S}_1, \mathbf{S}_2)$ as illustrated below. In contrast, for $q \neq 1$, PN integrations need to be initialized with either ξ, S and J at finite separation, or through $\kappa_\infty = \lim_{r\to\infty}\mathbf{S}\cdot\hat{\mathbf{L}}$ at infinitely large separation. One then needs to precession average S^2 using $\mathrm{d}S/\mathrm{d}t$ from equation (26) of [29] and numerically integrate for the evolution of J on $t_{\rm RR}$ according to equation (38) of that work.

2.2. Orbital-plane and spin precession

For $q \neq 1$ the precession dynamics are conveniently parametrized by S, but we have seen that in the equal-mass case S is constant and, hence, no longer suitable for this purpose. Instead, we consider φ' defined as the angle traced out relative to some reference value φ'_0 by the spin $\mathbf{S}_1$ in the plane orthogonal to the total spin $\mathbf{S}$; see figure 1. We can fix the reference value φ'_0 by defining [29]

$$\cos\varphi' = \frac{\hat{\mathbf{S}}_1\cdot\hat{\mathbf{S}}_\perp}{|\hat{\mathbf{S}}_1\times\hat{\mathbf{S}}|} = \frac{\hat{\mathbf{S}}_1\cdot[(\hat{\mathbf{S}}\times\hat{\mathbf{L}})\times\hat{\mathbf{S}}]}{|\hat{\mathbf{S}}_1\times\hat{\mathbf{S}}|\,|\hat{\mathbf{S}}\times\hat{\mathbf{L}}|}, \tag{2.8}$$

where $\hat{\mathbf{S}}_\perp$ is the unit vector perpendicular to $\mathbf{S}$ and $\mathbf{S}\times\mathbf{L}$. Note that the orientation of $\mathbf{S}_2$ in the same plane is automatically determined through this definition by closure of the triangle ($\mathbf{S}$, $\mathbf{S}_1$, $\mathbf{S}_2$). The angle φ' thus corresponds to rotations of $\mathbf{S}_1$ and $\mathbf{S}_2$ about $\mathbf{S}$. Using equations (7), (10), (28) and (29) of [29] together with the spin-precession equations (2.3) and (2.4) one can show that equation (2.8) implies

$$\frac{\mathrm{d}\,\cos\varphi'}{\mathrm{d}t} = \frac{1}{|\mathbf{S}_1\times\hat{\mathbf{S}}|}\left(\hat{\mathbf{S}}_\perp\frac{\mathrm{d}\mathbf{S}_1}{\mathrm{d}t}+\mathbf{S}_1\frac{\mathrm{d}\hat{\mathbf{S}}_\perp}{\mathrm{d}t}\right) \;\Rightarrow\; \frac{\mathrm{d}\varphi'}{\mathrm{d}t} = -\frac{3S}{r^3}\left(1-\xi\sqrt{\frac{M}{r}}\right)\leqslant 0, \tag{2.9}$$

where the last inequality is manifest for separations $r\geqslant M$, since $|\xi|<2S/M^2\leqslant 1$ for Kerr BHs with $\chi\leqslant 1$. We conclude that the angle φ' always evolves monotonically and $\cos\varphi'$ evolves periodically back and forth between -1 and $+1$. While the two spins precess about $\mathbf{S}$ with phase φ', the orbital plane precesses about $\mathbf{J}$ with frequency [28, 29]

$$\Omega_z = \frac{1}{4}\frac{M^{3/2}}{r^{5/2}}\sqrt{1+\frac{\xi M^2}{L}+\frac{S^2}{L^2}}\left(7-\frac{3}{2}\frac{M^2\xi}{L}\right). \tag{2.10}$$

It is interesting to note that the timescale of these two phenomena scale differently with the separation r. While the orbital plane precesses on $t\sim\Omega_z^{-1}\propto r^{5/2}$, the two spins precess about $\mathbf{S}$ on the longer time scale $t\sim\varphi'\mathrm{d}t/\mathrm{d}\varphi'\propto r^3$. This appears surprising at first glance since both powers enter the orbit-averaged spin-precession equations (2.3) and (2.4) and one would expect the shorter timescale to dominate both features. For generic $q\neq 1$ binaries, this is indeed the case; both, Ω_z^{-1} and $\varphi'\mathrm{d}t/\mathrm{d}\varphi'$, scale as $r^{5/2}$ [29]. The markedly different behaviour of $q=1$ binaries arises from a cancelation of all terms $\propto L\propto\sqrt{r}$ in the numerator on the right-hand side of equation (2.9). The leading order term $\propto r^{-5/2}$ thus drops out of the evolution of the two spins about $\mathbf{S}$, but remains present in the precessional motion of $\mathbf{S}$ and $\mathbf{L}$ about $\mathbf{J}$ as described by Ω_z of equation (2.10) where no such cancelation occurs.

2.3. Spin morphologies

The angle φ' is a valuable quantity to mathematically formulate the precession dynamics, but is not ideal for forming an intuitive picture.This is achieved more conveniently using instead the angles between the vectors $\mathbf{S}_1$, $\mathbf{S}_2$ and $\mathbf{L}$,

$$\cos\theta_1 = \hat{\mathbf{S}}_1\cdot\hat{\mathbf{L}}, \tag{2.11}$$

$$\cos\theta_2 = \hat{\mathbf{S}}_2\cdot\hat{\mathbf{L}}, \tag{2.12}$$

$$\cos\theta_{12} = \hat{\mathbf{S}}_\mathbf{1}\cdot\hat{\mathbf{S}}_\mathbf{2}, \tag{2.13}$$

and the azimuthal angle between the projections of the two spins onto the orbital plane

$$\cos\Delta\Phi = \frac{\hat{\mathbf{S}}_\mathbf{1}\times\hat{\mathbf{L}}}{|\hat{\mathbf{S}}_\mathbf{1}\times\hat{\mathbf{L}}|}\cdot\frac{\hat{\mathbf{S}}_\mathbf{2}\times\hat{\mathbf{L}}}{|\hat{\mathbf{S}}_\mathbf{2}\times\hat{\mathbf{L}}|}. \tag{2.14}$$

In general, all four angles, θ_1, θ_2, θ_{12} and $\Delta\Phi$, oscillate on the precessional timescale, while GW emission drives the secular evolution. In the unequal-mass case, the angles θ_1, θ_2 and θ_{12} evolve monotonically during each precession cycle (we define a cycle in this context to cover the evolution of φ' over an interval $\Delta\varphi' = \pi$), while the evolution of $\Delta\Phi$ follows either of three qualitatively different scenarios (see e.g. figure 3 of [29]):

(i) $\Delta\Phi$ can circulate spanning the full allowed range $[-\pi, \pi]$,
(ii) $\Delta\Phi$ can librate about 0, and never reaches $\pm\pi$,
(iii) $\Delta\Phi$ can librate about $\pm\pi$, and never reaches 0.

This behavior enables us to classify the precessional dynamics into *morphologies*. In general, the specific morphology of a binary is a function of the separation r: radiation reaction may cause a BH binary to transition from one morphology to another. These transitions can only happen if either $\cos\theta_1 = \pm 1$ or $\cos\theta_2 = \pm 1$ at some point during a precession cycle. At that moment, one of the spins is (anti-) aligned with $\mathbf{L}$ and $\Delta\Phi$ is not well defined; see equation (2.14).

The $q = 1$ case addressed here differs from this picture in some important aspects. The angles describing the directions of the spins are obtained from setting $q = 1$ in equations (10) of [29] and evaluating the corresponding scalar products which gives

$$\cos\theta_1 = \frac{1}{4S_1S^2}\Big[\xi M^2(S^2 + S_1^2 - S_2^2) + \sqrt{4S^2 - \xi^2M^4}\sqrt{S^2 - (S_1 - S_2)^2}\sqrt{(S_1 + S_2)^2 - S^2}\cos\varphi'\Big], \tag{2.15}$$

$$\cos\theta_2 = \frac{1}{4S_2S^2}\Big[\xi M^2(S^2 + S_2^2 - S_1^2) - \sqrt{4S^2 - \xi^2M^4}\sqrt{S^2 - (S_1 - S_2)^2}\sqrt{(S_1 + S_2)^2 - S^2}\cos\varphi'\Big], \tag{2.16}$$

$$\cos\theta_{12} = \frac{S^2 - S_1^2 - S_2^2}{2S_1S_2}, \tag{2.17}$$

$$\cos\Delta\Phi = \frac{\cos\theta_{12} - \cos\theta_1\cos\theta_2}{\sin\theta_1\sin\theta_2}. \tag{2.18}$$

We see that θ_{12} is constant while the angles θ_1 and θ_2 oscillate between the two extrema

$$\cos\theta_{1\pm} = \frac{1}{4S_1S^2}\Big[\xi M^2(S^2 + S_1^2 - S_2^2) \pm \sqrt{4S^2 - \xi^2M^4}\sqrt{S^2 - (S_1 - S_2)^2}\sqrt{(S_1 + S_2)^2 - S^2}\Big], \tag{2.19}$$

$$\cos\theta_{2\pm} = \frac{1}{4S_2S^2}\Big[\xi M^2(S^2+S_2^2-S_1^2) \mp\sqrt{4S^2-\xi^2M^4}\,\sqrt{S^2-(S_1-S_2)^2}\,\sqrt{(S_1+S_2)^2-S^2}\Big], \tag{2.20}$$

as φ' evolves monotonically between 0 and π during each precession cycle. For $q=1$, the boundaries $\theta_{1\pm}$ and $\theta_{2\pm}$ do not depend on either J or L, but only on the constants of motion ξ, S, S_1 and S_2. In contrast to the $q\neq 1$ case, they therefore do not vary on the radiation reaction timescale. This implies that the spin morphology, i.e. the qualitative evolution of $\Delta\Phi$, remains unchanged at all separations. Equal-mass binaries do *not* exhibit morphological transitions, which sets them qualitatively apart from their generic unequal-mass counterparts.

The three different morphologies are still present, however, in the (ξ, S; S_1, S_2) parameter space of equal-mass binaries. In particular, binaries in the two librating morphologies exist even at infinitely large separations ($r\to\infty$), while for $q\neq 1$ all binaries circulate in this limit. The main point is that a given binary never crosses the boundary between the different morphologies. These boundaries are given by the condition $\cos\theta_{i\pm}=\pm 1$ and a binary that happens to be sitting at such a point will sweep through an aligned configuration $\mathbf{S_i}\|\mathbf{L}$ during each and every precession cycle throughout its entire inspiral. The condition $\cos\theta_1=\pm 1$ can be solved for ξ as a function of S, yielding

$$\xi = \pm\frac{2S}{M^2}\frac{2S_1S(S^2+S_1^2-S_2^2)+[4S_1^2S_2^2-(S^2-S1^2-S_2^2)^2]|\cos\varphi'|\sqrt{\cos^2\varphi'-1}}{4S^2S_1^2+[4S_1^2S_2^2-(S^2-S1^2-S_2^2)^2](\cos^2\varphi'-1)}, \tag{2.21}$$

while $\cos\theta_2=\pm 1$ has solutions

$$\xi = \pm\frac{2S}{M^2}\frac{2S_2S(S^2-S_1^2+S_2^2)+[4S_1^2S_2^2-(S^2-S1^2-S_2^2)^2]|\cos\varphi'|\sqrt{\cos^2\varphi'-1}}{4S^2S_2^2+[4S_1^2S_2^2-(S^2-S1^2-S_2^2)^2](\cos^2\varphi'-1)}. \tag{2.22}$$

Real valued solutions only exist for the three discrete values $\cos\varphi'=0,-1,+1$. For $\cos\varphi'=0$, we obtain

$$\cos\theta_1=\pm 1 \quad\Rightarrow\quad \xi=\pm\frac{4S_1S^2}{M^2(S^2+S_1^2-S_2^2)}, \tag{2.23}$$

$$\cos\theta_2=\pm 1 \quad\Rightarrow\quad \xi=\pm\frac{4S_2S^2}{M^2(S^2-S_1^2+S_2^2)}. \tag{2.24}$$

It is straightforward to verify that these solutions violate the bound (2.2) and can be discarded as unphysical. On the other hand, the solutions for $|\cos\varphi'|=1$ (corresponding to $\theta_{i\pm}$ of equation (2.19) and (2.20))

$$\cos\theta_1=\pm 1 \quad\Rightarrow\quad \xi=\pm\frac{S^2+S_1^2-S_2^2}{S_1}, \tag{2.25}$$

$$\cos\theta_2=\pm 1 \quad\Rightarrow\quad \xi=\pm\frac{S^2-S_1^2+S_2^2}{S_2}, \tag{2.26}$$

fall into the allowed range (2.2). These configurations correspond to binaries for which the spin morphology is ill-defined during the entire inspiral and they mark the boundary between the different morphologies as we will discuss in more detail in the next section.

3. Results: a simple picture

In the previous section we have seen that the evolution of a quasi-circular equal-mass binary with fixed spin magnitudes χ_1, χ_2 is completely determined by the values of ξ and S which remain constant during the inspiral. The orbital angular momentum measures the binary separation and the total angular momentum J is given by equation (2.5). We can therefore graphically visualize the set of all binaries with given χ_1, χ_2 in the (S, ξ) configuration space and analyse the properties of a binary as a function of its location in this diagram. The resulting diagrams are shown in figure 2 for several representative choices of χ_1 and χ_2.

Since S and ξ are both constants of motion, BH binaries are stationary in these plots as they inspirals towards merger. Each panel in figure 2 therefore encompasses all equal-mass BH binary evolutions with given spin magnitudes χ_1 and χ_2.

The physically allowed region in the parameter space is determined by the constraint $\mathbf{S} = \mathbf{S_1} + \mathbf{S_2}$ and the limits (3.2) for ξ which gives us a total of four conditions

$$|S_1 - S_2| \leqslant S \leqslant S_1 + S_2, \tag{3.1}$$

$$-2S \leqslant \xi M^2 \leqslant 2S. \tag{3.2}$$

The resulting curves are shown as dotted lines in the top panel of figure 2. Note that the condition (3.2) for ξ can be shown to be equivalent to the constraint $\mathbf{S} = \mathbf{J} - \mathbf{L}$ for the magnitude S; in particular $\xi = 2S/M^2$ corresponds to $S = |J - L|$ and $\xi = -2S/M^2$ corresponds to $S = J + L$.

The four corners of the resulting allowed region in the (S, ξ) plane correspond to binaries with both spins (anti-) aligned with the orbital angular momentum (i.e. $\sin\theta_1 = \sin\theta_2 = 0$). More specifically, the top-right (bottom-right) corner maximizes (minimizes) ξ and, hence, correspond to both spins being aligned (antialigned) with $\mathbf{L}$. We refer to these binaries as *up–up* (**UU**) and *down−down* (**DD**), respectively. The left boundary of the allowed region minimizes S, so that the two spins $\mathbf{S}_1$ and $\mathbf{S}_2$ are antialigned with each other. The two left corners represent the corresponding maximum (minimum) in ξ where the larger (smaller) spin is aligned and the other spin antialigned with $\mathbf{L}$. We refer to these points as *up-down* or *down-up* (**UD/DU**). Since S is constant, all these four 'corner' configurations are stable under spin precession and phenomena like the *up-down* instability found in [45] do not occur for equal-mass binaries. Using equation (2) in that paper, one immediately sees that *both* instability thresholds $r_{\rm ud\pm}$ go to ∞ as $q \to 1$.

The angles of equations (2.11)–(2.14) describing the mutual orientation of $\mathbf{S_1}$, $\mathbf{S_2}$ and $\mathbf{L}$ are all constant for binaries located on the edge of the allowed region because all terms $\propto \cos\varphi'$ in equations (2.15) and (2.17) vanish for either $S = |S_1 \pm S_2|$ or $\xi = \pm 2S/M^2$. We note that for $S = S_1 + S_2$ the two spins are aligned with each other, so that $\Delta\Phi = 0$, while $\Delta\Phi = \pm\pi$ for the other cases $S = |S_1 - S_2|$ and $\xi = \pm 2S/M^2$. These configurations lying at the edge of the allowed region correspond to the spin–orbit resonances discovered in [44]. The three momenta $\mathbf{S_1}$, $\mathbf{S_2}$ and $\mathbf{L}$ share a common plane (i.e. $\sin\Delta\Phi = 0$) and jointly precess about $\mathbf{J}$ with fixed mutual directions. While for $q \neq 1$ such mutual directions undergo secular changes due to radiation reaction, they are truly constant for the $q = 1$ case examined here (i.e. they are independent of L). These are indeed the two families of resonant solutions identified in [44], characterized by either $\Delta\Phi = 0$ or $\Delta\Phi = \pm\pi$. The $\Delta\Phi = 0$ family runs from **UU** to **DD** along the right border where $S = S_1 + S_2$, while the $\Delta\Phi = \pm\pi$ family connects **UU** to **DD** along the bottom ($\xi = -2S/M^2$), left ($S = |S_1 - S_2|$) and top ($\xi = 2S/M^2$) borders.

Next, we consider the different spin morphologies which we display in figure 2 by color coding different areas in the parameter space. Through equations (2.15)–(2.18), we can regard

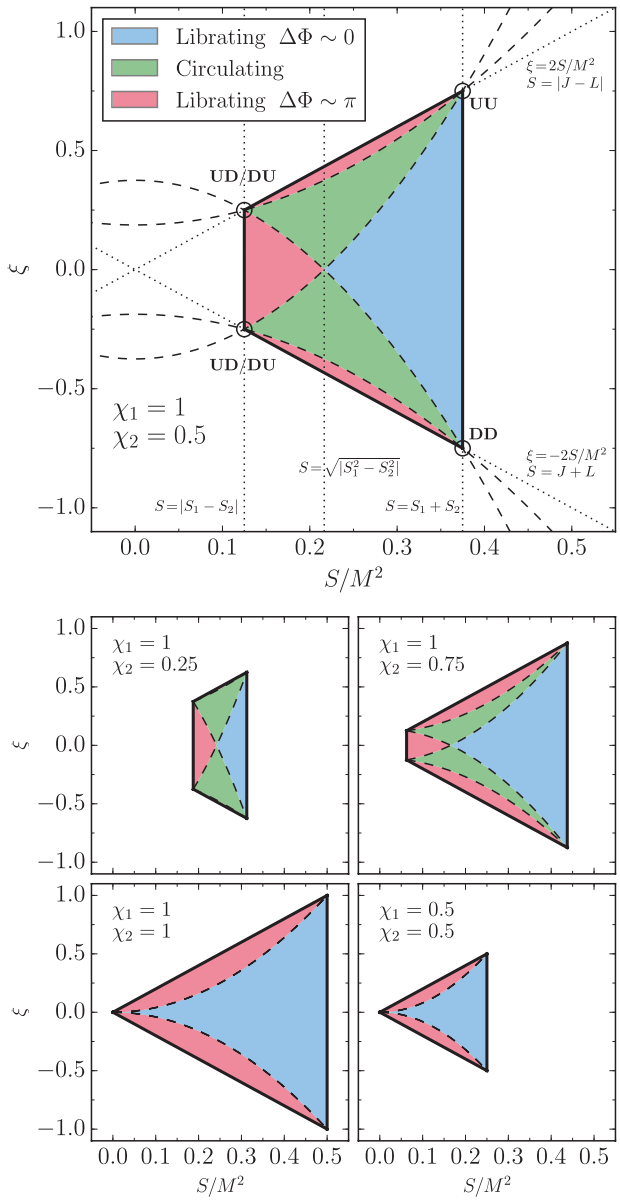

Figure 2. Configuration space of equal-mass BH binaries in the PN regime. Each binary is characterized by the two constants of motions S and ξ, reported on the x and y axes respectively. The various panels show the configuration space for different values of the dimensionless spin magnitudes χ_1 and χ_2. As expected, the panels are invariant under a relabelling of the binary constituents $(\chi_1, \chi_2) \to (\chi_2, \chi_1)$. The physically allowed region is given by the area inside the four lines $S = |S_1 + S_2|$ and $\xi = \pm 2S/M^2$, shown as dotted curves in the top panel. In each panel, we show the resulting boundaries as a solid thick line and they mark the spin–orbit resonances, while round circles at the four corners **UU**, **DD** and **UD/DU** mark binaries with both spins parallel to the orbital angular momentum. The spin morphology is encoded by the color of the shaded region and their boundaries are given by the dashed curves given by equations (2.25) and (2.26).

$\Delta\Phi$ as a function of $\cos\varphi'$. The three vectors $\mathbf{L}$, $\mathbf{S_1}$ and $\mathbf{S_2}$ are coplanar at $\cos\varphi' = \pm 1$, and therefore $\sin\Delta\Phi(\cos\varphi' = \pm 1) = 0$. A morphology boundary is defined by the discontinuous change of the function $\Delta\Phi(\cos\varphi')$ as the parameters S, ξ are varied a little. By equation (2.18), such a discontinuous change is only possible at $\sin\theta_1 \times \sin\theta_2 = 0$ which are precisely the solutions (2.25) and (2.26) shown as dashed parabolae in figure 2. We already know the behavior of the binaries on the edge of the physically allowed region, so that binaries located close to the edge boundaries librate about either $\Delta\Phi = 0$ (right; blue colored area in figure 2) or $\Delta\Phi = \pm\pi$ (bottom, left, top; red colored) as they approach the two families of resonant binaries where $\Delta\Phi = \text{constant} = 0, \pm\pi$. In the central regions (green), binaries circulate in the full range $\Delta\Phi \in [-\pi, \pi]$. Two of the four solutions (2.25) and (2.26) meet at each of the four corners where both spins are (anti-) aligned with the orbital angular momentum. These curves also intersect each other at the special configuration $S = \sqrt{|S_1^2 - S_2^2|}$ and $\xi = 0$, where two of the four *instantaneously aligned* configurations $\cos\theta_1 = \pm 1$, $\cos\theta_2 = \pm 1$ are touched during each precession cycle.

The fractions of the parameter space belonging to each morphology change with χ_1 and χ_2. In particular, more binaries are allowed to circulate (librate) if the two spin magnitudes are different (similar) to each other. In the limiting case $\chi_1 = \chi_2$ the four solutions of equation (2.25) and (2.26) correspond to only two distinct curves and binaries are not allowed to circulate.

It is trivial to show that the entire description we provided remains unchanged under the inversion $(\chi_1, \chi_2) \to (\chi_2, \chi_1)$. Finally, we point out that figure 2 in this paper should *not* be viewied as the $q = 1$ equivalent of figure 4 in [29]: that figure merely represents snapshots in the (S, ξ) parameter space of a set of binaries with the same value of J at a given separation r. Our figure 2 instead displays all binaries (with fixed χ_1, χ_2) over the entire PN inspiral.

4. Conclusions

We have analyzed the dynamics of spinning equal-mass BH binaries in light of the precession-averaged approach put forward in [28, 29]. The existence of an additional constant of motion, namely the magnitude of the total spin $S = |\mathbf{S_1} + \mathbf{S_2}|$, greatly simplifies the PN dynamics. For given spin magnitudes S_1 and S_2, PN inspirals can be labelled by couples (S, ξ), where ξ is the projected effective spin and is also a constant of motion. This entirely determines the binary evolution at 2PN order of the spin precession equations. The inspiral can be parameterized by the magnitude of the orbital angular momentum $L = m_1 m_2 \sqrt{r/M}$ and the magnitude of the total angular momentum $J = |\mathbf{L} + \mathbf{S}|$ is given by the analytic expression of equation (2.5). The spin tilts oscillate between the extrema given in equations (2.19) and (2.20) which do not depend on L and, thus, on the binary separation.

Together, these features let us picture the entire parameter space of equal-mass BH binaries using the diagrams of figure 2. While some features found for generic $q \neq 1$ binaries, such as the existence the two families of spin–orbit resonances, persist in the limit $q \to 1$, others turn out to be qualitatively different. In particular, the spin morphology (i.e. the qualitative evolution of the spin orientation on the precessional timescale) is constant throughout the inspiral and is uniquely determined by the values S and ξ of the binary in question. As hinted in [46, 47], future high-significance GW observations may provide direct measurements of the BH binary spin morphology. In the case of (nearly) equal-mass events, this would correspond to direct constraints on the spin directions at BH formation; in contrast, for the $q \neq 1$ case one needs to randomize over the precessional phase and evolve the observed configurations back to $r \to \infty$ [29].

Surprisingly, we found that precession of the BH spins and the orbital plane takes place on different timescales if $q = 1$: the former is $\propto r^3$ and thus longer than the $\propto r^{5/2}$ result found for (i) the orbital plane precession in the $q = 1$ case and (ii) for both precession time scales for generic $q \neq 1$ binaries. In principle, this finding may allow for a further timescale-averaging procedure, to separate the evolution of the BH spins relative to the orbital plane, and the evolution of the orbital plane in some inertial reference frame (see [48]).

The results presented in this paper have been implemented in the open-source python code PRECESSION, available at www.davidegerosa.com/precession [49]. In particular, the constancy of S and equation (2.5) for the evolution of J are exploited explicitly only if the code is run with $q = 1$. For any value of $q < 1$, the general formalism of [28, 29] is used. This has been found to provide accurate results for $0.005 \lesssim q \lesssim 0.995$ [49]. As a possible future extension of the code one may include the development of a hybrid approach combining the two formulations.

Acknowledgments

We thank Michael Kesden, Emanuele Berti and Richard O'Shaughnessy for several stimulating discussions. DG is supported by NASA through Einstein Postdoctoral Fellowship grant No. PF6-170152 awarded by the Chandra x-ray Center, which is operated by the Smithsonian Astrophysical Observatory for NASA under contract NAS8-03060. Additional support is acknowledged by NSF CAREER grants PHY-1151197 and PHY-1404569, the UK STFC, and the Isaac Newton Studentship of the University of Cambridge. JV was supported by the Bridgewater Summer Undergraduate Research Opportunities Programme and the Churchill College Small Grants fund at the University of Cambridge. This work has received funding from the European Union's Horizon 2020 research and innovation programme under the Marie Skłodowska-Curie grant agreement No 690904, from H2020-ERC-2014-CoG Grant No. 'MaGRaTh' 646597, from STFC Consolidator Grant No. ST/L000636/1, the SDSC Comet, PSC-Bridges and TACC Stampede clusters through NSF-XSEDE Award Nos. PHY-090003, the Cambridge High Performance Computing Service Supercomputer Darwin using Strategic Research Infrastructure Funding from the HEFCE and the STFC, and DiRAC's Cosmos Shared Memory system through BIS Grant No. ST/J005673/1 and STFC Grant Nos. ST/H008586/1, ST/K00333X/1. Figures were generated using the Python package MATPLOTLIB [50].

References

[1] Aasi J *et al* 2015 *Class. Quantum Grav.* **32** 074001
[2] Acernese F *et al* 2015 *Class. Quantum Grav.* **32** 024001
[3] Seoane P A *et al* 2013 arXiv:1305.5720
[4] Manchester R N *et al* 2013 *Publ. Astron. Soc. Aust.* **30** e017
[5] Kramer M and Champion D J 2013 *Class. Quantum Grav.* **30** 224009
[6] Jenet F *et al* 2009 arXiv:0909.1058
[7] Poisson E and Will C M 1995 *Phys. Rev.* D **52** 848–55
[8] Sathyaprakash B S and Schutz B F 2009 *Living Rev. Relativ.* **12** 2
[9] Campanelli M, Lousto C O and Zlochower Y 2006 *Phys. Rev.* D **74** 041501
[10] Penrose R 1969 *Nuovo Cimento Rivista Serie* **1** 252–76
[11] Wald R M 1997 *Black Holes, Gravitational Radiation and the Universe* ed B R Iyer (New York: Springer) pp 69–85
[12] Kidder L E 1995 *Phys. Rev.* D **52** 821–47
[13] Apostolatos T A, Cutler C, Sussman G J and Thorne K S 1994 *Phys. Rev.* D **49** 6274–97

[14] Gerosa D, Kesden M, Berti E, O'Shaughnessy R and Sperhake U 2013 *Phys. Rev.* D **87** 104028
[15] Rodriguez C L, Zevin M, Pankow C, Kalogera V and Rasio F A 2016 *Astrophys. J. Lett.* **832** L2
[16] Abbott B P *et al* 2016 *Astrophys. J. Lett.* **818** L22
[17] Rezzolla L 2009 *Class. Quantum Grav.* **26** 094023
[18] Kesden M, Sperhake U and Berti E 2010 *Phys. Rev.* D **81** 084054
[19] Hofmann F, Barausse E and Rezzolla L 2016 *Astrophys. J. Lett.* **825** L19
[20] González J A, Hannam M, Sperhake U, Brügmann B and Husa S 2007 *Phys. Rev. Lett.* **98** 231101
[21] Campanelli M, Lousto C O, Zlochower Y and Merritt D 2007 *Phys. Rev. Lett.* **98** 231102
[22] Kesden M, Sperhake U and Berti E 2010 *Astrophys. J.* **715** 1006–11
[23] Bohé A *et al* 2016 arXiv:1611.03703
[24] Khan S, Husa S, Hannam M, Ohme F, Pürrer M, Forteza X J and Bohé A 2016 *Phys. Rev.* D **93** 044007
[25] Damour T and Nagar A 2014 *Phys. Rev.* D **90** 044018
[26] Chatziioannou K, Klein A, Cornish N and Yunes N 2017 *Phys. Rev. Lett.* **118** 051101
[27] Peters P C 1964 *Phys. Rev.* **136** 1224–32
[28] Kesden M, Gerosa D, O'Shaughnessy R, Berti E and Sperhake U 2015 *Phys. Rev. Lett.* **114** 081103
[29] Gerosa D, Kesden M, Sperhake U, Berti E and O'Shaughnessy R 2015 *Phys. Rev.* D **92** 064016
[30] Pretorius F 2005 *Phys. Rev. Lett.* **95** 121101
[31] Baker J G, Centrella J, Choi D I, Koppitz M and van Meter J 2006 *Phys. Rev. Lett.* **96** 111102
[32] Campanelli M, Lousto C O, Marronetti P and Zlochower Y 2006 *Phys. Rev. Lett.* **96** 111101
[33] Pretorius F 2007 Binary black hole coalescence *Physics of Relativistic Objects in Compact Binaries: from Birth to Coalescence* ed M Colpi *et al* (New York: Springer)
[34] Centrella J, Baker J G, Kelly B J and van Meter J R 2010 *Rev. Mod. Phys.* **82** 3069–119
[35] Pfeiffer H P 2012 *Class. Quantum Grav.* **29** 124004
[36] Cardoso V, Gualtieri L, Herdeiro C A R and Sperhake U 2015 *Living Rev. Relativ.* **18** 1
[37] Sperhake U 2015 *Class. Quantum Grav.* **32** 124011
[38] Abbott B P *et al* 2016 *Phys. Rev.* X **6** 041014
[39] Abbott B P *et al* 2016 *Phys. Rev. Lett.* **116** 241102
[40] Abbott B P *et al* 2016 *Phys. Rev. Lett.* **116** 241103
[41] Abbott B P *et al* 2016 *Phys. Rev.* X **6** 041015
[42] Damour T 2001 *Phys. Rev.* D **64** 124013
[43] Racine É 2008 *Phys. Rev. D* **78** 044021
[44] Schnittman J D 2004 *Phys. Rev.* D **70** 124020
[45] Gerosa D, Kesden M, O'Shaughnessy R, Klein A, Berti E, Sperhake U and Trifirò D 2015 *Phys. Rev. Lett.* **115** 141102
[46] Gerosa D, O'Shaughnessy R, Kesden M, Berti E and Sperhake U 2014 *Phys. Rev.* D **89** 124025
[47] Trifirò D, O'Shaughnessy R, Gerosa D, Berti E, Kesden M, Littenberg T and Sperhake U 2016 *Phys. Rev.* D **93** 044071
[48] Zhao X, Kesden M and Gerosa D 2017 (in preparation)
[49] Gerosa D and Kesden M 2016 *Phys. Rev.* D **93** 124066
[50] Hunter J D 2007 *Comput. Sci. Eng.* **9** 90–5